UNIVERSITY OF CALIFORNIA
RIVERSIDE

Type I Interferon Signaling Differences Among Avian and Human Influenza A Virus Strains

A Thesis submitted in partial satisfaction
of the requirements for the degree of

Master of Science

in

Biomedical Sciences

by

Dania Lizet Amaya

June 2026

Thesis Committee:
Dr. Juliet Morrison, Chairperson
Dr. Milton Hamblin
Dr. Marcus Kaul

The Thesis of Dania Lizet Amaya is approved:

_____

_____

_____

Committee Chairperson

University of California, Riverside

Acknowledgements

To begin, I would like to thank Dr. Juliet Morrison for her mentorship, guidance, and support throughout my master's research and graduate studies. I would also like to thank Roksana Shirazi for her mentorship and advice that she provided me during the beginning stages of my graduate training and project development. I would also like to thank Dr. Hamblin for his support throughout my graduate studies at the University of California, Riverside School of Medicine in the Biomedical Sciences program. His guidance on research development, professional advice, and overall support helped ease my way through my graduate studies. Secondly, I would like to sincerely thank my undergraduate students, specifically Evan Ruiz and Pranav Hastak, for their hard work and dedication in helping me with my research. Their dedication to experimental work, troubleshooting, and good spirits helped when things did not work out during the experimental phase of my thesis, and without their help, my research would not have been possible. Lastly, I would like to sincerely thank the CA Wellness Foundation Pathway Programs Scholarship and the Kaloostian and Shirinian Scholarship for the 2024-2026 academic years for their financial support throughout my master's program. The generosity from these programs helped alleviate my financial burden associated with graduate school and allowed me to continue working on my master's thesis project. I would also like to thank Dr. Morrison's Startup Funds for supporting and funding my project during my time working in her laboratory. Thank you to everyone who has helped me in any way, all the connections I made during this program, and thank you for this opportunity!

Dedication

I would like to dedicate this thesis to my parents, who sacrificed so much for me to have the opportunity to seek higher education and to work towards a brighter future. Immigrating from Central America for a better future for their children is the greatest gift and sacrifice that I will always honor. Their hard work, dedication, determination, and most of all love influenced my work ethic and helped me become a better person, researcher, mentor, and woman. Without them, I would not be where I am today, and I am so thankful for their support. Most importantly, I dedicate this work to myself. All the sacrifices, hardships, long nights, and failures encountered throughout my journey were not easy, but I always found a way to persevere. As a first-generation Latina woman in STEM, the academic and personal endeavors I encountered tested my confidence and resilience. From failing classes in my undergrad and experiencing imposter syndrome, I never thought I could have the opportunity to participate in research, let alone create a research project. This opportunity has shaped and prepared me to embrace the challenges and to be kind to myself. Focusing on the present rather than anticipating the future has been a constant theme during graduate school, and I plan to continue this new mentality in every aspect of my life. Cada sacrificio tiene su recompensa, and I hope to soon enjoy the fruits of my labor. While I may not know what exactly my future career will be, I hope that God's plan will lead me to joy, purpose, and peace. I hope to continue embodying kindness, compassion, and open-mindedness in all aspects of my life. My experiences at the University of California, Riverside have shaped me, and I hope to carry these lessons forward in hopes of contributing to a kinder and better future for others!

Table of Contents

List of Figures

List of Tables

Abstract

Highly Pathogenic Avian Influenza (HPAI) H5N1-virus strains have been reported in the United States, circulating in cattle farms and ultimately causing a spillover from cattle to humans. The emergence of this new strain has heightened public health concerns about its pathogenicity, transmissibility, and interactions with the innate immune system in humans. Influenza A Virus (IAV) employs multiple strategies to evade the host's innate immune system, including HA-mediated degradation of type I interferon (IFN-I) receptors during active infection.

This study aims to compare and investigate whether the HA protein of the current circulating HPAI H5N1 IAV enhances IFN-I receptor (IFNAR1) degradation in A549 pulmonary cells and, if so, what mechanisms are being utilized to promote receptor degradation and enhanced viral pathogenicity. Protein sequence alignments of A/Texas/37/2024 (H5N1), A/Washington/2148/2025 (H5N5) H5 HA proteins, and A/California/04/2009 (H1N1) H1 HA protein were done to compare the conserved and divergent sequence regions of the IAV strains. In addition, the replication kinetics of A/Vietnam/1203/2004 H5N1 (referred to as HALo) and A/Netherlands/602/2009 H1N1 (referred to as NL09) IAV were conducted in A549 cells that had been exposed to IFN-I at different time points and concentrations using plaque assay analysis. Lastly, FLAG-tagged HA proteins were transfected and used to compare their IFNAR1 degradation using Western blot analysis.

The data suggest that the protein sequence alignments between the two H5 HA proteins showed highly conserved regions, while comparing both H5 HA proteins to the H1 HA protein demonstrated divergence and potential differences in biochemical functions and pathogenicity. As for the HALo (H5N1) and NL09 (H1N1) IAV, the replication kinetics experiments demonstrate distinct replication patterns between HALo and NL09; however, no statistically significant difference was seen following IFN-I at different time points and concentrations. Lastly, HA plasmid transfections were successful in 293T cells; however, due to nonspecific binding in the Western blot analysis, further investigation of IFNAR1 degradation was not explored.

Collectively, while the findings are preliminary and require further exploration, this work serves as a foundation for future experiments and can help investigate the mechanisms underlying HA-induced IFNAR1 degradation and overall viral pathogenesis of the currently circulating HPAI H5N1 IAV.

Introduction

As of 2024, numerous spillovers of highly pathogenic avian influenza (HPAI) H5N1 influenza A virus (IAV) have occurred across the United States, raising concerns about potential outbreaks related to human infection (Centers for Disease Control and Prevention [CDC], 2024). After devastating marine bird and mammal populations, H5N1 IAV has now spread to cattle, poultry, and humans, raising urgent public health concerns (Eisfeld et al., 2024). Numerous states across the United States, specifically in the

southwest, have reported HPAI H5N1 infection in cattle, chickens, and barn cats, which ultimately impacted the dairy production of these farms and also highlighted the deaths of many wild birds around these farms (DeWeerdt et al., 2025). While influenza viruses have historically been reported to infect avian and feline hosts, infections in bovine hosts have been rare and have attracted the attention of many farmers, veterinarians, and public health departments in infected states (DeWeerdt et al., 2025). As a result of this, a spillover to humans from cattle in Texas, USA, was reported: a dairy farm worker was infected with HPAI H5N1 and presented with conjunctivitis, subconjunctival hemorrhage, and other respiratory symptoms (Uyeki et al., 2024).

There are four subtypes of Influenza viruses: Influenza A (IAV), B (IBV), C (ICV), and D (IDV). These four subtypes are members of the family *Orthomyxoviridae*, and each strain infects myriad hosts (Mostafa et al., 2018). The genome of this virus contains eight negative-sense single-stranded RNA segments, which encode three polymerase-encoding segments along with accessory viral proteins (PB1, PB2, PB1-F2, PA, and PA-X), hemagglutinin (HA), neuraminidase (NA), nucleoprotein (NP), matrix proteins-encoding segments (M1 and M2), and nonstructural proteins-encoding segments (NS1 and NEP) (Mostafa et la., 2018). Humans are primarily infected with the IAV, which also includes the HPAI H5N1 strain that was transmitted from cattle to humans in Texas.

In California alone, 38 human HPAI H5N1 cases have been confirmed from poultry and dairy farm workers, with the most recent on January 14, 2025 (California Department of

Public Health [CPHD], 2024). During the 2024–2025 influenza season, a trivalent vaccine that protects against three different influenza strains- an influenza A (H1N1) virus, an influenza A (H3N2) virus, and an influenza B/Victoria virus was administered to the public and targeted dairy and poultry farm workers, but while effective against H1N1 IAV, it failed to halt HPAI H5N1 IAV spread (CDC, 2024). Usually, HPAI H5N1 does not bind well to the α-2,6 sialic acid (Sia) cell receptors in the upper respiratory tract of most people, as this type of IAV prefers the α-2,3 sialic acid receptors found in avian and bovine species (Mostafa et al., 2018). Humans also express α-2,3-linked sialic acid receptors in the lower respiratory tract, primarily in the alveoli of the lungs. The importance and significance of these receptors became evident following the emergence of A/Hong Kong/156/97 (H5N1), demonstrating that an avian virus could directly infect humans without the need for an intermediate host (Walther et al., 2013). In avian species, their α-2,3-linked sialic receptors are predominantly located within their enteric tract, as the receptor distribution corresponds to the dominant sialic acid linkage utilized by the avian influenza viruses (Liu et al., 2022). Similarly, bovine species α-2,3 sialic receptors have been detected in their mammary glands. The relevance of their receptor distribution has been further confirmed and supported by mouse model studies that demonstrate transmission of HPAI H5N1 IAV from infected lactating mice to uninfected, suckling offspring (Ríos et al., 2024; Eisfeld et al., 2024). However, recently this has changed as the current circulating Texas HPAI H5N1 strain acquired notable mutations that allowed the HA protein of this strain to successfully bind and recognize the α-2,6 receptors in humans, noting the preference switch of receptors for this virus (Lin et al., 2024; Schmidt

et al., 2025). Due to the ability of HPAI H5N1 to evade host immune responses, evade host antiviral defenses, and enhance its viral pathogenicity, understanding how the immune system responds to severe viral infection may help reduce viral transmission and further spread of the virus. (Cao et al., 2017; Octaviani et al., 2025).

The innate immune system is the first line of defense for the human body, and there are many factors of this system that help fight off viral infections and help alleviate symptoms in humans. Type I Interferons (IFN-I or IFN-α/β) belong to the class II cytokine family, and their mechanism of action elicits antiviral activity when secreted from any nucleated cell, especially plasmacytoid dendritic cells (pDCs) (Lazear et al., 2019; Foley et al., 2016). IFN-I binds to a heterodimeric receptor (IFNAR), which is made up of two subunits, IFNAR1 and IFNAR2. Once bound to the receptor, this dimerization activates TYK2 and JAK1 kinases, which then phosphorylate STAT1 and STAT2, causing them to bind to IRF9 and form the ISGF3 complex. The ISGF3 complex translocates to the nucleus, where it binds to the interferon-stimulated response elements (ISREs), leading to interferon-stimulated gene (ISG) transcription. Once these genes are transcribed and translated, they elicit the expression of more ISGs to help promote antiviral responses in cells (Lazear et al., 2019). While IFN-I elicits antiviral activity when viral particles are detected in a host, other systems also contribute to this antiviral activity and can also play a dual role in aiding the virus to replicate. Interferon III (IFN-III/IFN-λ) shares similar antiviral properties and contributes to viral recognition, triggering the production of ISGs encoding antiviral functions within infected and

surrounding cells (Major et al., 2020). IFN-III binds a heterodimeric receptor composed of IFNLR1 and IL10Rβ, but uses the JAK/STAT signaling molecules as IFN-I (Lazear et al., 2019). A key characteristic of IFN-λ that distinguishes it from IFN-α/β is that its receptor, IFNLR, is mainly expressed in epithelial cells; therefore, it allows for a more localized antiviral protection at the site of infection without promoting unnecessary proinflammatory responses like IFN-α/β (Major et al., 2020). While IFN-λ has a more localized anti-inflammatory response in epithelial cells, HPAI H5N1 replicates robustly in the human respiratory tract and is more efficient at evading the IFN-α/β immune response (Turnball et al., 2025). Since Type I and III Interferon signaling pathways overlap, it is uncertain whether HPAI H5N1 viruses can exhibit IFN-λ receptor degradation in the same manner as it does with IFN-α/β. Further research is needed to confirm whether HPAI H5N1's methods of evading the innate immune response include IFN-λ evasion or if this interferon is playing a different role during active infection.

IAVs have adopted numerous methods of evading the innate immune system to promote their replication, which then leads to severe infections within the host. One method by which H1N1 IAV viruses can evade the host's innate immune system is by degrading the IFNAR1 receptor in cells, which is currently not fully understood (Xia et al., 2016). It has been reported that H1N1 IAV can interact with the IFN-I system to downregulate the expression levels of IFNAR1 during an active infection, leading to unregulated cellular responses. With the degradation of IFNAR1 by H1N1 IAV, it begs the question of whether HPAI H5N1 IAV can elicit interferon receptor degradation or similar

anti-interferon responses. With confirmation that the Texas HPAI H5N1 IAV strain acquired amino acid mutations to allow its HA protein to recognize and bind to α-2,6 sialic acid cell receptors (Lin et al., Bayoumi et al.) and that H1N1 IAV can degrade IFNAR1 as a way to evade the innate immune system (Xia et al.), then further research needs to be applied to the Washington HPAI H5N5, as this newly isolated circulating strain can elicit similar behavior as the Texas HPAI H5N1 and California H1N1.

In this study, I will be investigating whether the HA protein of the current circulating HPAI H5N1 IAV enhances IFN-1 receptor degradation in A549 cells and, if so, what mechanisms are being utilized to promote receptor degradation and enhanced viral pathogenicity. Understanding HPAI H5N1 IAV's replication and interactions with the innate immune system is critical to assessing its severity and developing strategies to control transmission before the next outbreak.

Materials and Methods

Cells

MDCK-PA and A549 cells were cultured and grown in Dulbecco's Modified Eagle's Medium (DMEM) + GlutaMAX-I with 10% Fetal bovine serum and 1% Penicilin / Streptomycin; all cell types were incubated at 37 °C, 5% CO_2, and checked every 3-5 days for passaging. 293T cells were cultured and grown in DMEM. Cells were obtained from the ATCC and Morrison Laboratory at the University of California, Riverside.

Viruses

A/Netherlands/602/2009 (H1N1), NL09, and an attenuated strain of A/Vietnam/1203/2004 (H5N1), HALo, described in Steel et al., were used to infect A549 and MDCK-PA during experiments to measure replication kinetics and test the pathogenicity of various viral titers. A/Vietnam/1203/2004 (H5N1) IAV was used in this study because this strain was engineered to include a deletion of the HA polybasic cleavage site, which allows it to be used for biosafety level 2+ work (Park et al., 2006). Viruses were obtained from the Hai Laboratory at the University of California, Riverside.

Viral Infections

MDCK-PA cells at 95-100% confluence were seeded in 12-well plates at a seeding density of 1 x 10^6 cells per well in DMEM (1X) + GlutaMAX-I, prepared with 10% FBS and 1% Penicillin/Streptomycin. Cells were incubated overnight at 37 °C, 5% CO_2. Cells were washed with 1 mL of Phosphate Buffer Solution (PBS). Once washed, cells were inoculated with 200 µL of HALo and NL09 in 10-fold dilutions. Cells were incubated for 1 hour with 20-minute rocking intervals; the viral inoculum was then aspirated, and cells were plated at a 1:1:1 ratio overlay of 2X DMEM-BSA solution, 1.5% Oxoid Agar, and Trypsin-TPCK. Plates were fixed and stained with 10% Crystal Violet on day 3 for HALo and day 4 for NL09, and their viral titers were calculated 1 day post-staining.

Growth Curve

A549 cells were cultured in 2 x T175 flasks, and when 95 - 100% confluence was reached, cells were seeded in 12 x 35 mm plates with a seeding density of 1 x 10^6 cells per plate. Plates were incubated at 37 °C, 5% CO_2, for both growth curves to double overnight. In the first growth curve, A549 cells were infected with either HALo or NL09 IAV in the presence or absence of IFN-β. For the second growth curve, A549 cells were treated with either HALo or NL09 Influenza A virus, then exposed to three different concentrations of IFN-β (10, 100, or 1000 units/mL) to evaluate a dose-dependent effect on viral replication. Viral inoculum master mixes were made with VBS and kept at an MOI of 10. For both growth curves, cells were washed with PBS, then infected with 200 µL of viral inoculum, followed by a 1-hour incubation period with 20-minute rocking intervals. After infection, the viral inoculum was aspirated, and cells were overlaid with 2 mL of either DMEM-BSA or DMEM-BSA enriched with IFN-β. The control medium contained 14 mL DMEM-BSA and 14 µL of Trypsin-TPCK, while the interferon treatment medium additionally contained 1.4 µL IFN-β. Plate samples were collected at designated time points from 0 to 24 hours post-infection and frozen at -80 °C to later assess viral replication kinetics and determine viral titers via plaque assay.

Interferon Concentrations and Inoculum Preparation

IFN-β was purchased from PBL Sciences and had an activity concentration of 5.1 x 10^6 units/mL. Concentrations to measure interferon activity with HALo and NL09 were inspired by Hsiang et al. for the growth curve experiments. Based on this paper, the three

concentrations of IFN-β were 10 units/mL, 100 units/mL, and 1000 units/mL. Control plates contained either HALo or NL09 titers without interferon. All concentrations of IFN-β were serially diluted and prepared in Virus Buffer Solution (VBS). To achieve the 3 listed IFN-β concentrations, 10 µL of IFN-β was mixed with 990 µL VBS to reach 5.1 x 10^4 (1000 units/mL final concentration). Then, 100 µL was taken from that vial and mixed into 900 µL of VBS to make 5.1 x 10^3 units/mL (100 units/mL final concentration). The last dilution involved mixing 100 µL from the 5.1 x 10^3 units/mL solution with 900 µL of VBS to reach 5.1 x 10^2 units/mL (10 units/mL final concentration). Once the dilutions were made, 275 µL from each IFN-β dilution tube was added to the corresponding tube containing 14 mL of DMEM-BSA and 14 µL Trypsin-TPCK media mixture. Once the mixtures were made, 2 mL of each treatment group was aliquoted onto the 24 x 35 mm A549 cell plates of the second growth curve.

Protein Sequence Alignment and Plasmid Construct

Influenza A Virus HA gene sequences for Texas, Washington, and California were found in the NCBI GenBank. Each gene sequence for all three strains was selected based on a complete, uncleaved HA protein. Once identified, each sequence underwent BLAST to ensure that there were no ambiguous strains. After running BLAST on a separate document, the FLAG gene sequence was also searched and added to an area of the HA strain genes where there was no stop codon, so that the gene can be read continuously during DNA transcription. However, when inputting FLAG, the stop codon of the original HA gene has to be moved to the end of the FLAG sequence to indicate the stop

of transcription. Plasmid constructs were designed with Twist Bioscience. Each HA plasmid construct included regulatory elements that helped facilitate efficient expression in mammalian cells, which included: Cytomegalovirus (CMV) promoter and Chicken β-Actin promoter. Other vector components included Ampicillin resistance (ampR) for bacterial selection, Puromycin resistance cassette for mammalian selection, and ColE1 origin of replication to ensure high-copy plasmid propagation in *E. coli*. To ensure efficient cloning, restriction enzyme site analysis was screened with NEBcutter. HA sequences were screened to identify restriction sites that were not present in the HA coding region. Compatible restriction enzyme sites, like EcoRI_Nhel and HindIII_BamHI, were selected and included as flanking sites to ensure directional cloning, while preserving the insert. If other restriction enzyme sites were detected in the sequence, then other restriction enzymes were selected to ensure proper cloning.

DNA Transformation in *E. coli*

XC1 cells were defrosted from the -80 °C freezer, thawed on ice, and 30 µL of E. coli aliquots were distributed to 3 micro-centrifuge tubes placed on ice. While the tubes were on ice, 2 µL of IAV Hemagglutinin (HA) plasmid DNA (Texas, Washington, and California strains) was added to each tube and mixed gently. The tubes were kept in the ice bucket for 5 minutes for plasmid uptake. Cells were heat-shocked at 42 °C for 45 seconds and immediately placed back on ice. While on ice, 450 µL of SOC media was added to each tube. Tubes were shaken on their side for 1 hr to increase bacterial growth at room temperature. After an hour, with the flame on, 100 µL of each HA bacteria tube

was spread onto an Ampicillin agar plate. After spreading the bacteria, the plates were stacked and placed in an incubator at 37 °C overnight. After the overnight incubation, individual colonies formed and were selected for further growth. In a conical tube, 20 mL of LB Broth was aliquoted, and 20 µL of 100 mg/mL Ampicillin was added with the flame on for the starter culture. From the starter culture, 2 mL was aliquoted into three 15 mL tubes labeled with the HA strain. With a sterile pipette tip, the largest isolated colony from each plate was selected and added into their corresponding LB broth tube. Once selected, the culture tubes were shaken at 37 °C with a shaking speed of 250 rpm for 6 hours. During the shaking period, three 1L flasks were prepared by dissolving 3.75 g of LB Broth powder in 150 mL of Milli-Q water. Once mixed, the flasks were autoclaved and left to cool completely before adding 150 µL of 100 mg/mL Ampicillin. After the 6-hour shaking period, with the flame on, 500 µL of each bacterial culture was aliquoted into their corresponding 1L LB Broth + Ampicillin flask. Each flask was covered with foil and incubated at 37 °C with a shaking speed of 250 rpm for 12-16 hours.

DNA Plasmid Purification

After the 12-16-hour shaking for the three 1L HA bacteria flasks, each bacterial culture was collected into three 50 mL conical tubes. The bacterial cultures were centrifuged at 3,400 g for 10 minutes at 20°C. The supernatant was discarded, which resulted with bacterial pellets that would be used for DNA purification. The HA plasmid purification was done following the ZymoPure Plasmid Maxiprep manufacturer's instructions. Before purifying any DNA from the bacterial pellets, 88 mL of 95-100% Ethanol was added to

23 mL of ZymoPURE Wash 2 concentrate before use. ZymoPURE P2 and ZymoPURE Binding Buffer were incubated at 30 - 37 °C for 10-20 minutes and mixed by inversion. ZymoPURE P1 (Red) was stored in a 4 °C fridge until ready for use.

The bacterial cell pellets were mixed together for each HA strain by splitting the total amount of 14 mL of ZymoPURE P1 (Red) across the 3 tubes. Each HA strain (TX, WA, and CA) was mixed into one labeled 50 mL conical tube and vortexed until fully dissolved. Once fully dissolved, each bacterial sample was combined with 14 mL of ZymoPURE P2 (blue) and mixed by gently inverting six times. Samples were then left at room temperature for 2-3 minutes until the lysis was complete, indicated by a clear, purple color. Following the lysis step, 14 mL of ZymoPURE P3 (yellow) was added to each conical tube and mixed thoroughly by gentle inversion. Each tube was inverted an additional 5 times until the samples turned completely yellow, indicating neutralization and allowing a precipitate to form.

Each HA lysate was clarified using a ZymoPURE Zyringe Filter-X by pouring the mixture in and then attaching a plug to the top of the filter. Then, each filter device was placed over three clean 50 mL conical tubes, and then left for the lysate to sit for 5-8 minutes to facilitate precipitate separation. The Luer Lock plug from the bottom of the syringes was removed, and the lysates were pushed through the filter to yield approximately 35 mL of cleared lysate. If 35 mL of lysate was not collected, then the ZymoPURE Binding Buffer volume was adjusted according to the manufacturer's

instructions in the back of the manual. To the 35 mL of lysate, 14 mL of ZymoPURE Binding Buffer was added to the cleared lysate and mixed thoroughly by inverting the tube 8 times.

To the ZymoPURE Vacuum manifold, three ZymoPURE Spin V-PX Column Assemblies were attached and labeled according to the HA strain. With the vacuum off, all samples were loaded into the columns, then the vacuum was turned on to allow the samples to pass through the column completely. The 50 mL Reservoir of the Zymo-Spin V-PX Column Assembly was discarded, then 10 mL of ZymoPURE Wash 1 was added to each Zymo-Spin V-PX Column Assembly with the vacuum on until completely passed through. With the vacuum off, 10 mL of ZymoPURE Wash 2 was added to each column and then passed through completely with the vacuum on. This step was repeated twice, but for the second wash, the vacuum was left on for an additional 2 minutes after the liquid passed through completely to remove any residual wash buffer.

Once the washing steps were done, each HA Zymo-Spin V-PX column was placed in a collection tube, then centrifuged at 16,000 × g for 1 minute to remove any remaining wash buffer. The columns were transferred to three clean 1.5 mL microcentrifuge tubes, and 400 µL of ZymoPURE Elution Buffer was added directly to the column matrix. The elution buffer was left in the matrix for 2 minutes, then centrifuged at 16,000 × g for 1 minute.

Lastly, to ensure that the DNA was free of any residual endotoxins, the spin column eluates (roughly 400 µL) were placed in three more clean 1.5 mL microcentrifuge tubes, left in the spin column for 2 minutes, then centrifuged at 10,000 × g for 1 minute. Each HA sample was then tested with a NanoDrop Spectrophotometer for its DNA ng/µL final concentration.

SDS-PAGE and Western Blot

293T cells were plated in a 6-well plate with a seeding density of 1 x 10^6 cells per well with DMEM without antibiotics and incubated overnight in 5% CO_2, 37 °C. Cells were transfected with HA-encoding plasmids from Texas (TX), Washington (WA), and California (CA) strains, along with a GFP control. 1 µg/µL of each DNA was diluted in 250 µL Opti-MEM I Reduced Serum Medium without Serum and combined with 10 µL of Lipofectamine 2000 diluted in 250 µL of Opti-MEM. The mixture was incubated for 5 minutes, then added dropwise to the cells. Plates were incubated, then the media was replaced 4 - 6 hours post-transfection. Cells were then incubated for 24 - 72 hours until ready to measure cell transgene expression.

Transfection of DNA was confirmed at the 48-hour mark by checking the GFP fluorescence in the control plate. Media was aspirated, then cells were washed with PBS, scraped, and collected in microcentrifuge tubes and centrifuged at 4 °C, 6000 × g (rcf) for 5 minutes. PBS was aspirated, then cell pellets were lysed with TAP Lysis buffer mixed with 4µL β-Mercaptoethanol and 1 Protease Inhibitor pill. Cell lysate tubes were

vortexed well, and samples were left on ice for 10 minutes. Tubes were centrifuged at 4 °C at maximum speed, and 200 µL of lysate was mixed with 40 µL of 5X Laemmli Sample Buffer. Tubes were punctured at the lid with a needle for venting, then denatured at 90 °C for 5 minutes before gel electrophoresis; the remaining whole cell extract was saved at 20 °C until ready for use.

SDS-PAGE gels were made with equal parts of Resolving Gel, Stacking Solution, 10% APS, and TEMED. Once gels were made in glass cassettes and solidified, gels were run for 1 hour, then transferred onto Methanol-activated Polyvinylidene Difluoride (PVDF) membranes. The membrane was stacked with 1x Transfer Buffer Solution-treated filter paper and placed in the Transblot Turbo Transfer machine for 7 minutes at 1.3A, 20 V. The PVDF membrane was placed in a tray and blocked in 5% BSA Blocking Buffer for 1 hour at room temperature. After the hour passed, the PVDF membrane was washed 5 times for 3 minutes each with 1X TBST Washing Buffer. After blocking, 10 µL of rabbit anti-FLAG-rabbit primary antibody (1:1000) in 10 mL 5% BSA Blocking Buffer was added to the membrane and incubated overnight at 4 °C. PDVF membrane was washed 5 times with 1X TBST Washing Buffer, then incubated at room temperature for 1 hour with 1 µL of Goat-α-rabbit IgG (H+L) HRP secondary antibody (1:20000) in 20 mL of 5% BSA Blocking Buffer. The membrane was washed as previously described after the post-incubation hour, then treated with 5 mL of Luminol Reagent. Membranes were visualized using chemiluminescence via the ChemiDoc Touch Imaging System.

Graphing and Statistical Analysis

All graphs were generated using Microsoft Excel and Google Workspace. All statistical analyses were performed using XLMiner Analysis ToolPak in Google Sheets. Figures were assembled using Google Workspace.

Results

Protein Sequence Comparison between A/Texas/37/2024 (H5N1), A/Washington/2148/2025 (H5N5), and A/California/07/2009 (H1N1)

Before conducting experiments comparing the pathogenicity of the different IAV strains, protein sequence alignments were performed on uncleaved hemagglutinin (HA) protein sequences to identify similarities and differences among the strains. Two H5 HA protein strains isolated from Texas and Washington were compared with one H1 HA protein strain that was isolated in California using the NCBI BLAST tool.

Understanding how the interferon signaling pathway responds to active IAV infections is key to determining whether viral strains elicit different responses. IAV has been shown to interfere with multiple components of the IFN-I pathway, thereby promoting viral propagation and evading antiviral host responses (Figure 1).

When comparing the Washington H5 protein with the California H1 protein, both protein sequences demonstrated a 63% identity match and 78% positive match between both sequences (Figure 2A). These findings indicate that both proteins share similar

biochemical functions and conserved sites in their sequences to elicit similar chemical responses. However, in further downstream positions of the protein alignments, there are more evident amino acid substitutions for the California H1 HA sequence. When constructing the HA protein plasmid, synonymous amino acids were incorporated to not disrupt the overall function of this protein alignment for further analysis.

Another protein sequence alignment was done with Texas H5 HA and California H1 HA to see if there are any differences or similarities between the two H5 HA proteins and the H1 HA protein. Similar to the Washington H5 HA protein, the Texas H5 HA protein showed a 62% identity and 78% positive match to the California H1 HA protein (Figure 2B). Since the first human-infecting bovine H5N1 case in the United States was isolated from Texas in early 2024, this highlighted a mutation in the HA protein that may allow this strain of HPAI H5N1 to have potential interspecies transmission. As a result of this, the concern of potential human-to-human transmission could result in another influenza pandemic, which is why the H5 HA protein of the Texas strain was compared to the H1 HA protein of the California IAV strain to highlight their similarities and differences (Lin et al. 2024). Overall, these results suggest that both H5 HA protein sequences demonstrate similar differences when compared to the California H1 HA IAV strain.

When comparing the Texas H5 HA and Washington H5 HA protein sequences, both H5 HA protein sequences share a 98% identity and 98% positive match, which indicates the same amino acids are present in their sequences and strongly suggests that they share

similar, but not identical, functions and contain conservative substitutions to distinguish their differences (Figure 2C). As a result of these conserved biochemical properties in the H5 HA IAV proteins, strains have reportedly been tested for their replication and pathogenicity in different animal models such as mice and ferrets to monitor transmissibility as well as receptor specificity for different host interactions (Eisfeld et al. 2024). Differences in pathogenicity as well as host interactions can be influenced by specific amino acid substitutions or additional viral factors that would need to be further explored outside of their protein sequences.

Establishing a Model System to Measure IAV and IFN-β Activity

To establish an *in vitro* lung model system to compare the pathogenicity between the seasonal, NL09 (H1N1), and avian, HALo (H5N1), IAV, A549 cells were used to study the replication kinetics between the two viruses to have a better understanding of their characteristics when exposed to the IFN-I signaling pathway, specifically IFN-β (Mostafa et al., 2025; Jiao et al., 2020). HALo (H5N1) IAV was used for this study since this strain was engineered from a fatal human case to include the deletion of the HA polybasic cleavage site, which allows for this variant to be used for biosafety level 2+ work (Park et al., 2006). For each time point, plates were infected with both strains of IAV, plus an IFN-β-treatment group that was added with IAV over the course of 24 hours. For the HALo and NL09 IAV control groups, A549 cells were not treated with IFN-β, and cells were only infected with each virus at an MOI of 10 to assess feasible replication kinetics

over 24 hours. The samples were frozen, thawed, and analyzed by plaque assay using MDCK-PA cells to determine and compare viral titers.

In the HALo control group, the viral titers increased during the early time points of the experiment, demonstrating a greater than 10-fold increase between 0 and 2 hours-post infection (hpi) (Figure 3A). The maximum viral titer for HALo IAV control plate reached 3.60×10^6 PFU/mL at 12 hpi, then plateaued. In comparison, HALo-infected cells that were treated with IFN-β demonstrated a delayed viral titer increase during the earlier time points; however, at 4 hpi, the viral titers began to increase and peaked at 2.65×10^6 PFU/mL at 12 hpi. The results of the IFN-β-treated group are comparable to the HALo control group. At the exponential level, the data showed similar replication trends between both groups, demonstrating that viral replication occurred in the earlier time points and plateaued later during the infection period (Figure 3B). No statistical differences were seen between the control and IFN-β-treated plates over the 24 hours (Table 1). Overall, the data suggest that HALo IAV had similar replication kinetics overall when comparing the control group with the IFN-β-treated group.

As for NL09 (H1N1) IAV, the earlier time points of the experiment showed a different result in comparison to the HALo (H5N1) IAV. The replication kinetics of this IAV strain were slower in the earlier time points of the control group, but increased in the later time points. In the earlier NL09 control time points, the viral titers decreased and later peaked at 12 hpi with 4.77×10^5 PFU/mL. Viral titers decreased at 24 hpi, suggesting either viral

plateau or cell death from prolonged viral exposure. In comparison to the NL09-infected cells treated with IFN-β, viral replication took place in the earlier time points and peaked at 2.42 x 10^7 PFU/mL before plateauing in the later stages of the infection (Figure 3C). Exponential analysis of the data demonstrated a delayed or slowed replication time at the earlier time points, gradually increased at 12 hpi, and then decreased towards the end of the experiment (Figure 3D). No statistical differences were observed between the control and IFN-β-treated plates over the 24 hours (Table 2). Overall, these data suggest that NL09 IAV replication differed from HALo and had a delayed replication during the early stages of infection, prior to viral titers peaking at the later time points before plateauing.

Overall, the data suggest that both viruses differed in their replication kinetics as well as their viral titers. Previous studies have also confirmed that H5N1 IAV is more efficient with its viral replication than H1N1 IAV. Avian H5N1 IAV elicits more IFN-β production at 4 hpi, and this pattern of production also decreases at later time points of the infection in comparison to seasonal H1N1 IAV (Tong et al. 2012). Along with this, previous papers have also confirmed that low viral titers of H5N1, both *in vitro* and *in vivo* model systems, succumb to infection, and different virulence factors elicited from H5N1 IAV strains are more pathogenic than H1N1 IAV strains (Mostafa et al. 2025). While the IFN-β treatment did not result in statistically significant antiviral effects, this model system serves as a good foundation to test the interactions between influenza A virus and type-I interferon-associated antiviral effects.

Testing and Comparing Different Interferon-β Concentrations against HALo (H5N1) and NL09 (H1N1) Influenza A Virus

With the model system from the previous figure suggesting that IFN-β could inhibit two different strains of IAV, the next step was to determine whether different concentrations of IFN-β would impact this outcome and, if so, whether the results from the two different strains of IAV would be similar, different, or inconclusive.

HALo IAV viral titers were variable when treated with varying concentrations of IFN-β during 24 hours. In the earlier time points, specifically 4 hpi, there was a large peak for the 10 units/mL of IFN-β, and the other IFN-β concentrations also peaked earlier in the experiment (Figure 4A-B). In contrast, the control group data demonstrated low viral titer in the earlier time points and plateaued at 12 hpi along with the IFN-β concentrations. No statistical differences were seen between the control and IFN-β concentration plates over the 24 hours (Table 1). This can indicate that robust viral replication was lacking in the control group and that a true antiviral state was not entirely achieved in the IFN-β groups. A sudden peak for the 10 units/mL IFN-β could have resulted from an inaccurate count or overall viral efficiency, meaning that the virus was able to overtake the treatment and cause more infection.

When comparing the HALo control data with the different IFN-β concentrations in Figure 4A-B, the cytokine treatment appeared not to affect the overall HALo IAV virus infection. With a cytokine response being measured at 4 hpi, this indicates that the

cytokine treatment is more time-dependent in the earlier stages of the infection, demonstrating a higher viral titer of HALo in the MDCK-PA cells, matching the plates containing numerous plaques in the cell monolayer. (Lee et al. 2018, Tong et al. 2012). However, there was no clear indication of whether the dose-dependent manner of the IFN-β fully inhibited the HALo IAV replication and overall viral efficacy. This suggests that HALo adapted to the A549 cell host responses during the growth curve to allow better viral propagation, which was then quantified in the plaque assays to show a low antiviral state (Muñoz-Moreno et al. 2021).

In comparison, NL09 IAV demonstrated variable responses for the different IFN-β concentrations when comparing replication to the control group (Figure 4C-D). For all groups, the data demonstrated low viral titers in the earlier time points of infection, but at 4 hpi, all groups had a sudden peak in viral titers. The highest viral titer for the groups was at 12 hpi for the 1000 units/mL of IFN-β group with 1.01×10^7 PFU/mL. Along with this, the 10 units/mL of IFN-β also had this elevated viral titer at 24 hpi, despite having variable viral replications in the earlier time points. No statistical differences were seen between the control and IFN-β-treated plates over the 24 hours (Table 2). This could suggest that in the earlier time points, 10 units/mL of IFN-β did elicit an antiviral effect to protect the cells from NL09 IAV infection; however, the effect must not have been for long, since the viral titers began to increase drastically at 24 hpi.

Overall, these results may suggest that the IFN-β inhibition was minimal with the HALo IAV and inconsistent with the NL09 IAV. The overall dose-dependent effects were variable and led to a more time-dependent effect between the virus and interferon concentrations. Further experiments would need to be conducted to determine whether a dose-dependent addition of IFN-β can elicit a stronger antiviral effect within the cells, since interferon responses are highly nonlinear and small differences during the initiation phase could have different effects for downstream antiviral responses (Rivera et al. 2024).

HA Protein Expression of Texas (A/Texas/37/2024(H5N1)), Washington (A/Washington/2148/2025(H5N5)), and California (A/California/07/2009(H1N1)) to Measure IFNAR1 Degradation

While measuring and comparing replication kinetics and pathogenicity between HALo (H5N1) and NL09 (H1N1) IAV, another objective of this study was to measure the IFNAR degradation and to determine which HA protein was more efficient at doing so. Previous studies have shown that IAV antagonizes IFN-I signaling by promoting IFNAR1 degradation. During infection, IFNAR1 undergoes phosphorylation and ubiquitination, while expression of viral HA proteins has been shown to facilitate these cellular processes and overall reduce IFN-I antiviral responses (Xia et al. 2016).

To measure this, 293T cells were transfected with Texas (A/Texas/37/2024(H5N1)), Washington (A/Washington/2148/2025(H5N5)), and California

(A/California/07/2009(H1N1)) FLAG-tagged HA-plasmids along with GFP serving as the control. The 293-T cell transfections were successful at the 48-hour mark, as evidenced by the bright green cells of the GFP control (Figure 5A). Cells were then lysed and prepared for SDS-PAGE, transferred, and blotted with 1:1000 primary anti-FLAG-rabbit antibody and 1:20000 Goat-α-rabbit secondary antibody to detect all 3 HA proteins.

Western blot analysis detected all 3 HA protein bands, which appeared in the 75 kDa range of the ladder, confirming the molecular weight of the HA proteins (Figure 5B). Texas (H5N1) and California (H1N1) IAV demonstrated stronger bands in comparison to the Washington (H5N5) IAV band. However, nonspecific binding was observed in the control lane, GFP protein, which had a faint band present around the 75 kDa range, suggesting a false positive Western blot. As a result of this, the blot was not used to test for IFNAR1 degradation.

Another Western blot was performed using a new Goat-α-rabbit IgG (H+L) HRP secondary antibody at the same dilution ratio as previously described (Figure 5C-D). After the 1 hr secondary antibody incubation, the membranes were stained, and nonspecific binding was present once again in both membranes. Despite there being stronger bands for all three HA proteins, these false positive results would not permit IFNAR1 degradation to be tested. Further analysis would need to be performed to explore the reason for repeated nonspecific binding bands appearing in the control lane or if

adding a positive control would help minimize the nonspecific binding. Overall, the western blots remained inconclusive, and IFNAR1 degradation was not tested due to these results.

Discussion

The purpose of this study was to investigate whether the hemagglutinin (HA) protein of the current circulating HPAI H5N1 IAV enhances IFN-I-receptor degradation in an *in vitro* lung model system using A549 cells and, if so, what mechanisms are being utilized to promote receptor degradation and enhanced viral pathogenicity.

Understanding the replication mechanism of IAV and how it triggers the innate immune system, like IFN-I, to elicit antiviral responses to protect the host is key, since the HA protein utilizes multiple methods of evading this system to promote severe infection (Xia et al., Muñoz-Moreno et al.). Protein sequence comparisons between Texas (H5N1) H5 HA and Washington (H5N5) H5 HA demonstrated a high degree of sequence similarity, while still containing variable sequence sites in comparison to the California (H1N1) H1 HA protein. The data suggest that even with conserved sequence sites within the HA proteins, strain-specific amino acid mutations still contribute to the overall strain difference and variation in viral pathogenicity and host interactions. Overall, the HA protein sequence analysis confirmed the overall similarities and differences between the HA protein sequences of the strains, which can serve as a tool to identify variable pathogenic characteristics of the strains.

Investigating the interactions between H5N1 and H1N1 IAV in the presence of IFN-β activity using viral growth curves in A549 cells was critical to understanding whether antiviral activity would hinder the virus's replication and pathogenesis based on time and varying IFN-β concentrations. When comparing the viral replication kinetics between HALo and NL09, the data demonstrated that the HALo IAV control group had more efficient viral replication than the NL09 IAV control group. While the IFN-β-treated plates of both virus groups demonstrated variable responses across the time points, there was no statistically significant difference between the control and IFN-β-treated groups. Along with this, varying IFN-β concentrations over 24 hours resulted in inconsistent effects on the HALo and NL09 replication kinetics during the growth curve, which suggests that the antiviral responses elicited during these experiments were inconclusive. Further investigation would need to be conducted to understand their relationship.

Along with comparing the replication kinetics of HALo and NL09, another aim of this study was to measure and compare IFN-1-receptor degradation with 3 HA IAV proteins to see which was more effective. Texas H5 HA, Washington H5 HA, and California H1 HA FLAG-tagged plasmids, along with GFP as a control, were transfected into 293T cells, lysed at the 48-hour mark, and then transferred to PVDF membranes for Western blot incubation to measure HA presence in each sample and later used for IFNAR1 degradation detection. However, non-specific binding resulted in false-positive Western blot results, which highlights the need for further assay optimization before conducting experiments to test for IFNAR1 degradation detection in the membranes. While the

Western blots remained inconclusive, this allows for future experiments to be modified to avoid nonspecific binding and allow for IFNAR1 detection.

Several limitations arose during this study, which included limited time for experimental replication and limited access to materials for certain experiments. These limitations contributed to the variability across the time and dose-dependent IFN-β-treatment growth curve datasets. Additional biological replicates, extended time points to measure the full effect of IFN-β, and further optimization of the Western blot conditions, like utilizing positive controls for the FLAG-tagged proteins, would help reduce the variability of these experiments to understand the relationship between HA viral proteins and IFN-Is.

Overall, the data were inconclusive, and future directions would be required to enhance and optimize the foundational experiments that were established. While the findings are preliminary and require further exploration, this work serves as a foundation for future experiments and can help investigate the mechanisms underlying HA-induced IFNAR1 degradation and overall viral pathogenesis of the currently circulating HPAI H5N1 IAV.

References

1. Bayoumi, M., Barre, R. S., Escobedo, R. A., Shivanna, V., Jackson, N., Ye, C., … Martinez-Sobrido, L. (2025). Identification of amino acid residues in polymerase PB2 responsible for differential replication and pathogenicity of avian influenza virus H5N1 isolated from human and cattle in Texas, US. Emerging Microbes & Infections, 14(1). https://doi.org/10.1080/22221751.2025.2542247

2. "Bird Flu." Ca.gov, 2024, www.cdph.ca.gov/Programs/CID/DCDC/pages/Bird-Flu.aspx.

3. Centers for Disease Control and Prevention. "Key Facts about Seasonal Flu Vaccine." Influenza (Flu), 17 Sept. 2024, www.cdc.gov/flu/vaccines/keyfacts.html.

4. CDC. "CDC A(H5N1) Bird Flu Response Update October 11, 2024." Avian Influenza (Bird Flu), 2024, https://www.cdc.gov/bird-flu/spotlights/h5n1-response-10112024.html

5. Cao, Y., Huang, Y., Xu, K. et al. Differential responses of innate immunity triggered by different subtypes of influenza A viruses in human and avian hosts. BMC Med Genomics 10 (Suppl 4), 70 (2017). https://doi.org/10.1186/s12920-017-0304-z

6. DeWeerdt, Sarah. "Could Tracking Animals' Health Help to Avert the Next Pandemic?" *Nature*, 17 Dec. 2025, https://doi.org/10.1038/d41586-025-03602-7

7. Eisfeld, A.J., Biswas, A., Guan, L. et al. Pathogenicity and transmissibility of bovine H5N1 influenza virus. Nature 633, 426–432 (2024). https://doi.org/10.1038/s41586-024-07766-6

8. Foley, John F. "Interfering with Interferons." Science Signaling, vol. 9, 2016, p. ec30, https://doi.org/10.1126/scisignal.aaf4271.

9. Hsiang T, Zhao C, Krug RM. 2009. Interferon-Induced ISG15 Conjugation Inhibits Influenza A Virus Gene Expression and Replication in Human Cells. J Virol83:.https://doi.org/10.1128/jvi.01667-08

10. Jiao P, Fan W, Cao Y, Zhang H, Tian L, et al. (2020) Robust induction of interferon and interferon-stimulated gene expression by influenza B/Yamagata lineage virus infection of A549 cells. PLOS ONE 15(4): e0231039. https://doi.org/10.1371/journal.pone.0231039

11. Lazear, Helen M., John W. Schoggins, and Michael S. Diamond. "Shared and Distinct Functions of Type I and Type III Interferons." *Immunity*, vol. 50, no. 4, 2019, pp. 907–923. Elsevier, https://doi.org/10.1016/j.immuni.2019.03.025.

12. Lee, A. J., and A. A. Ashkar. "The Dual Nature of Type I and Type II Interferons." *Frontiers in Immunology*, vol. 9, 2018, p. 2061, https://doi.org/10.3389/fimmu.2018.02061.

13. Lin, Ting-Hui, et al. "A Single Mutation in Bovine Influenza H5N1 Hemagglutinin Switches Specificity to Human Receptors." *Science*, vol. 386, 2024, pp. 1128–1134, https://doi.org/10.1126/science.adt0180.

14. Liu, M., Huang, L.Z.X., Smits, A.A. et al. Human-type sialic acid receptors contribute to avian influenza A virus binding and entry by hetero-multivalent interactions. Nat Commun 13, 4054 (2022). https://doi.org/10.1038/s41467-022-31840-0

15. Major Jack et al. "Type I and III Interferons Disrupt Lung Epithelial Repair during Recovery from Viral Infection." Science, vol. 369, 2020, pp. 712–717, https://doi.org/10.1126/science.abc2061.

16. Man-Seong. Park, J. Steel, A. García-Sastre, D. Swayne, & P. Palese, Engineered viral vaccine constructs with dual specificity: Avian influenza and Newcastle disease, Proc. Natl. Acad. Sci. U.S.A. 103 (21) 8203-8208, https://doi.org/10.1073/pnas.0602566103.

17. Mi, Z., Ma, Y. & Tong, Y. Avian influenza virus H5N1 induces rapid interferon-beta production but shows more potent inhibition of retinoic acid-inducible gene I expression than H1N1 in vitro. Virol J 9, 145 (2012). https://doi.org/10.1186/1743-422X-9-145

18. Mostafa, A.; Abdelwhab, E.M.; Mettenleiter, T.C.; Pleschka, S. Zoonotic Potential of Influenza A Viruses: A Comprehensive Overview. Viruses 2018, 10, 497. https://doi.org/10.3390/v10090497

19. Mostafa, A., Barre, R. S., Allué-Guardia, A., Escobedo, R. A., Shivanna, V., Rothan, H., … Martínez-Sobrido, L. (2025). Replication kinetics, pathogenicity and virus-induced cellular responses of cattle-origin influenza A(H5N1) isolates from Texas, United States. Emerging Microbes & Infections, 14(1). https://doi.org/10.1080/22221751.2024.2447614

20. Muñoz-Moreno, R., Martínez-Romero, C., and García-Sastre, A. "Induction and Evasion of Type-I Interferon Responses during Influenza A Virus Infection." *Cold Spring Harbor Perspectives in Medicine*, vol. 11, no. 10, 2021, p. a038414, https://doi.org/10.1101/cshperspect.a038414.

21. Octaviani, C.P., Huang, P., Bi-Hung, P. et al. Superior replication, pathogenicity, and immune evasion of a Texas dairy cattle H5N1 virus compared to a historical avian isolate. Sci Rep 15, 8797 (2025). https://doi.org/10.1038/s41598-025-93493-5

22. Ríos Carrasco M, Gröne A, van den Brand JMA, de Vries RP.2024.The mammary glands of cows abundantly display receptors for circulating avian H5 viruses. J Virol98:e01052-24.https://doi.org/10.1128/jvi.01052-24

23. Rivera-Cardona J, Kakuturu N, Rowland EF, Teo QW, Thayer EA, et al. (2024) Seasonal influenza A virus lineages exhibit divergent abilities to antagonize interferon induction and signaling. PLOS Pathogens 20(12): e1012727. https://doi.org/10.1371/journal.ppat.1012727

24. Schmidt, Charles. "The Quest to Hatch a Bird-Flu Vaccine." Nature, 17 Dec. 2025, www.nature.com/articles/d41586-025-03612-5, https://doi.org/10.1038/d41586-025-03612-5.

25. Steel J, Lowen AC, Pena L, Angel M, Solórzano A, Albrecht R, Perez DR, García-Sastre A, Palese P. Live attenuated influenza viruses containing NS1 truncations as vaccine candidates against H5N1 highly pathogenic avian influenza. J Virol. 2009 Feb;83(4):1742-53. doi: 10.1128/JVI.01920-08. Epub 2008 Dec 10. PMID: 19073731; PMCID: PMC2643794.

26. Turnbull, M.L., Zakaria, M.K., Upfold, N.S. et al. The potential of H5N1 viruses to adapt to bovine cells varies throughout evolution. Nat Commun 16, 11042 (2025). https://doi.org/10.1038/s41467-025-67234-1

27. Uyeki, Timothy M, et al. “Highly Pathogenic Avian Influenza A(H5N1) Virus Infection in a Dairy Farm Worker.” New England Journal of Medicine/ the New England Journal of Medicine, vol. 390, no. 21, 3 May 2024, https://doi.org/10.1056/nejmc2405371.

28. Walther T, Karamanska R, Chan RWY, Chan MCW, Jia N, et al. (2013) Glycomic Analysis of Human Respiratory Tract Tissues and Correlation with Influenza Virus Infection. PLOS Pathogens 9(3): e1003223. https://doi.org/10.1371/journal.ppat.1003223

29. Xia C, Vijayan M, Pritzl CJ, Fuchs SY, McDermott AB, Hahm B.2016.Hemagglutinin of Influenza A Virus Antagonizes Type I Interferon (IFN) Responses by Inducing Degradation of Type I IFN Receptor 1. J Virol90:.https://doi.org/10.1128/jvi.02749-15

Figures

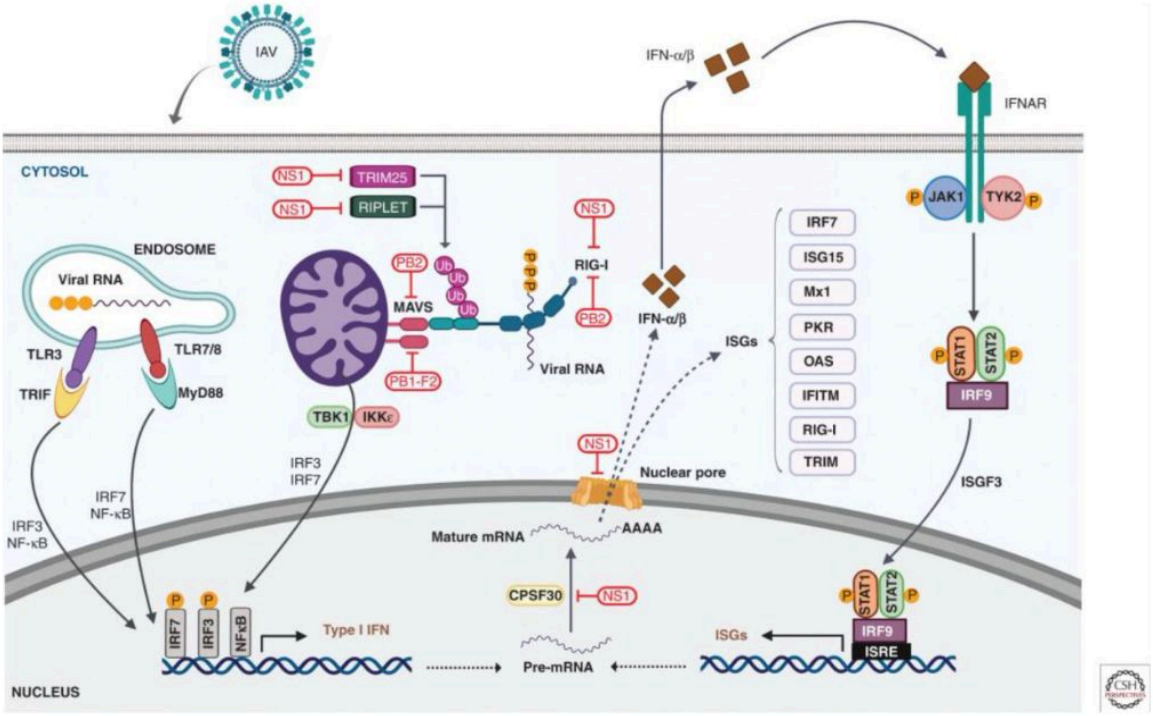

Figure 1. Type I Interferon Immune Response to Influenza A Virus Schematic Signaling Pathway Schematic overview of Innate Immune Response and Evasion strategies upon Influenza A virus infection, adapted from Muñoz-Moreno et al.

A Washington vs California

NW Score	Identities	Positives	Gaps
1987	358/569(63%)	445/569(78%)	5/569(0%)

```
Query  1    MENI-VLLLATVSLVKSDQICIGYHANNSTEQVDTIMEKNVTVTHAQDILEKTHNGKLCD  59
            M+ I V+LL T +   +D +CIGYHANNST+ VDT++EKNVTVTH+ ++LE  HNGKLC
Sbjct  1    MKAILVVLLYTFATANADTLCIGYHANNSTDTVDTVLEKNVTVTHSVNLLEDKHNGKLCK  60

Query  60   LNGVKPLILKDCSVAGWLLGNPMCDEFIRVPEWSYIVERANPANDLCYPGSLNDYEELKH  119
            L GV PL L  C++AGW+LGNP C+       WSYIVE  +  N  CYPG   DYEEL+
Sbjct  61   LRGVAPLHLGKCNIAGWILGNPECESLSTASSWSYIVETPSSDNGTCYPGDFIDYEELRE  120
```

B Texas vs California

NW Score	Identities	Positives	Gaps
1974	354/569(62%)	444/569(78%)	5/569(0%)

```
Query  1    MENI-VLLLAIVSLVKSDQICIGYHANNSTEQVDTIMEKNVTVTHAQDILEKTHNGKLCD  59
            M+ I V+LL   +   +D +CIGYHANNST+ VDT++EKNVTVTH+ ++LE  HNGKLC
Sbjct  1    MKAILVVLLYTFATANADTLCIGYHANNSTDTVDTVLEKNVTVTHSVNLLEDKHNGKLCK  60

Query  60   LNGVKPLILKDCSVAGWLLGNPMCDEFIRVPEWSYIVERANPANDLCYPGSLNDYEELKH  119
            L GV PL L  C++AGW+LGNP C+       WSYIVE  +  N  CYPG   DYEEL+
Sbjct  61   LRGVAPLHLGKCNIAGWILGNPECESLSTASSWSYIVETPSSDNGTCYPGDFIDYEELRE  120
```

C Texas vs Washington

NW Score	Identities	Positives	Gaps
2975	554/567(98%)	559/567(98%)	0/567(0%)

```
Query  1    MENIVLLLAIVSLVKSDQICIGYHANNSTEQVDTIMEKNVTVTHAQDILEKTHNGKLCDL  60
            MENIVLLLA VSLVKSDQICIGYHANNSTEQVDTIMEKNVTVTHAQDILEKTHNGKLCDL
Sbjct  1    MENIVLLLATVSLVKSDQICIGYHANNSTEQVDTIMEKNVTVTHAQDILEKTHNGKLCDL  60

Query  61   NGVKPLILKDCSVAGWLLGNPMCDEFIRVPEWSYIVERANPANDLCYPGSLNDYEELKHM  120
            NGVKPLILKDCSVAGWLLGNPMCDEFIRVPEWSYIVERANPANDLCYPGSLNDYEELKH+
Sbjct  61   NGVKPLILKDCSVAGWLLGNPMCDEFIRVPEWSYIVERANPANDLCYPGSLNDYEELKHL  120
```

Figure 2. Protein Sequence Alignment Comparison of Hemagglutinin (HA) Influenza A Virus Strains (**A**) Washington (A/Washington/2148/2025(H5N5) vs California (A/California/07/2009(H1N1), (**B**) Texas (A/Texas/37/2024(H5N1) vs California (A/California/07/2009(H1N1), and (**C**) Texas (A/Texas/37/2024(H5N1) vs Washington (A/Washington/2148/2025(H5N5). Number of residues (identities), similar residues (positives), and gaps are shown for each comparison.

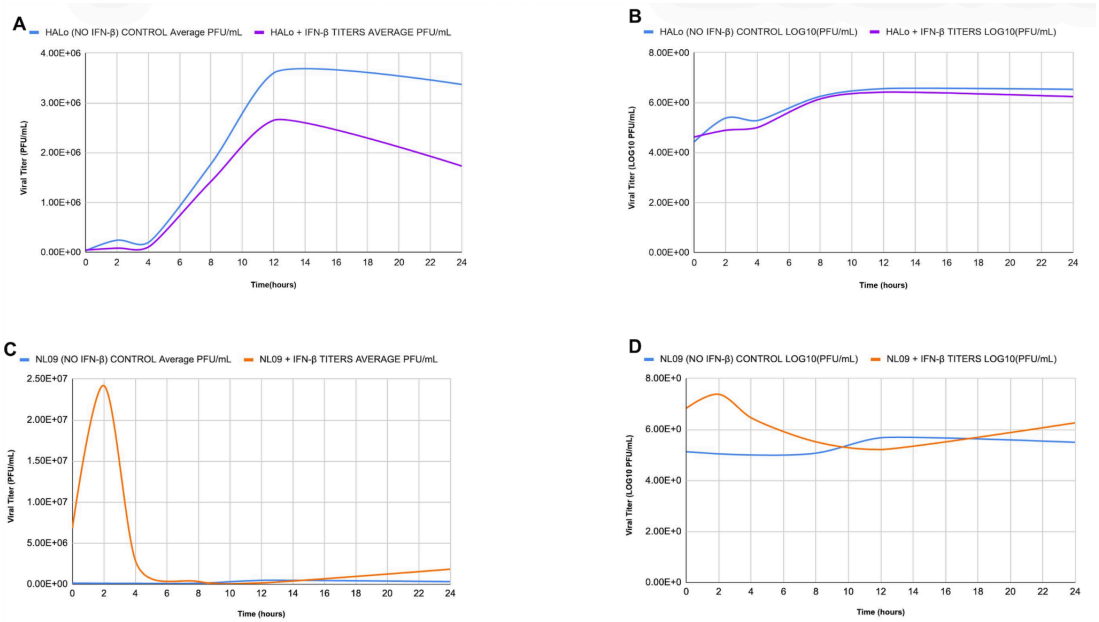

Figure 3. **Analysis of Replication Kinetics of HALo (H5N1) and NL09 (H1N1) Influenza A Virus in the Presence or Absence of IFN-β Treatment** (**A**) Linear growth curve analysis of A/Vietnam/1203/2004 (HALo, H5N1) viral replication from A549 cells under control and IFN-β treated plates over a 24 hour infection period (**B**) Exponential analysis of HALo viral titers shown in panel A, (**C**) Linear growth curve analysis of NL09 (H1N1) viral replication from A549 cells under control and IFN-β treated plates over a 24 hour infection period, and (**D**) Exponential analysis of NL09 viral titers shown in panel C.

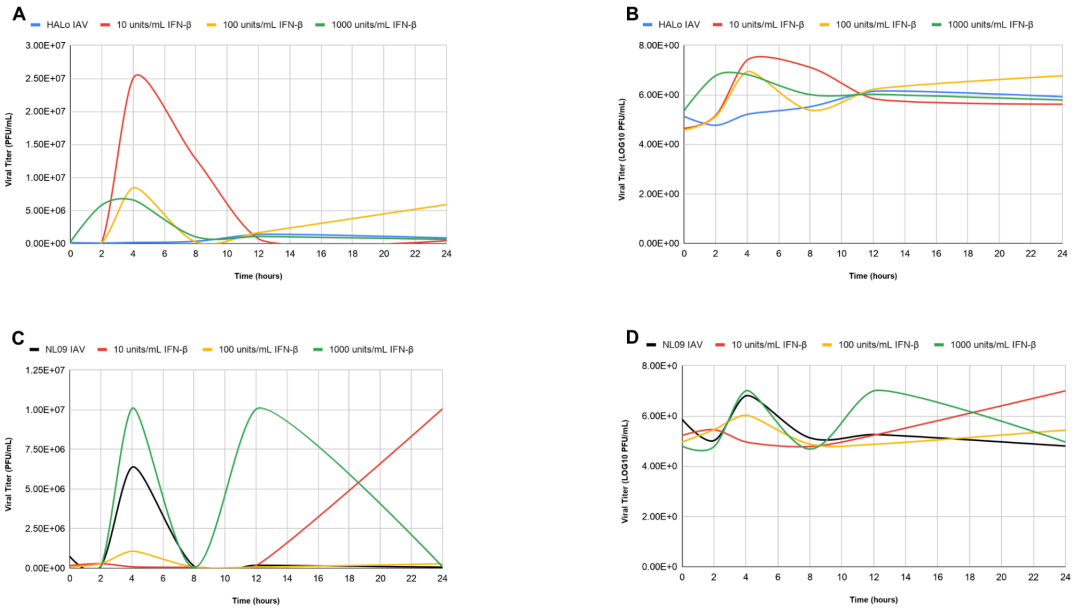

Figure 4. **Replication Kinetics Effects of HALo (H5N1) and NL09 (H1N1) Influenza A Virus at Different Concentrations of IFN-β Treatment** (**A**) Linear growth curve analysis of A/Vietnam/1203/2004 (HALo, H5N1) viral replication from A549 cells under control and varying IFN-β concentrations over a 24 hour infection period (**B**) Exponential analysis of HALo viral titers shown in panel A, (**C**) Linear growth curve analysis of NL09 (H1N1) viral replication from A549 cells under control and varying IFN-β concentrations over a 24 hour infection period, and (**D**) Exponential analysis of NL09 (H1N1) viral titers shown in panel C.

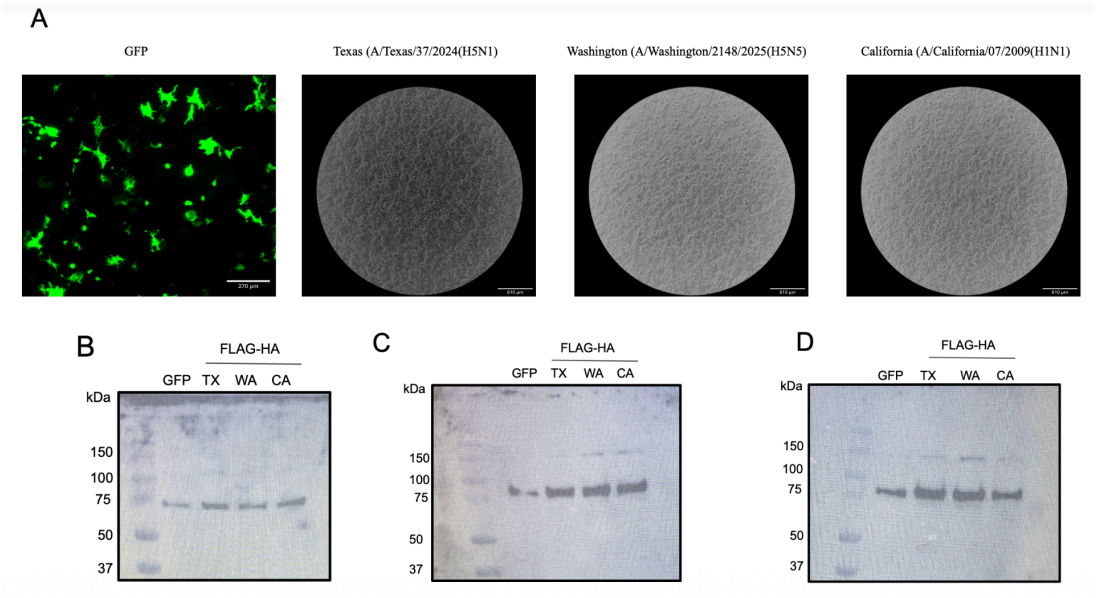

Figure 5. **293T Cell Transfection and Western Blot of FLAG-tagged HA-plasmids for Texas, Washington and California** (**A**) Fluorescence images of GFP and FLAG-tagged Influenza A virus HA proteins in transfected 293T cells (**B**) First Western Blot analysis of GFP (control), Texas (A/Texas/37/2024(H5N1), Washington (A/Washington/2148/2025(H5N5), and California (A/California/07/2009(H1N1), (**C-D**) Repeated Western Blot to evaluate nonspecific binding.

Tables

Table 1: Statistical Analysis of HALo and IFN-β Growth Curve Experiments					
Figure	**Timepoint**	**Comparison**	**Statistical Test**	***p-value***	**Statistic**
Fig. 3B	0 hpi	Growth Curve 1: HALo Control vs IFN-β	Welch's *t*-test	0.293	—
Fig. 3B	2 hpi	Growth Curve 1: HALo Control vs IFN-β	Welch's *t*-test	0.374	—
Fig. 3B	4 hpi	Growth Curve 1: HALo Control vs IFN-β	Welch's *t*-test	0.265	—
Fig. 3B	8 hpi	Growth Curve 1: HALo Control vs IFN-β	Welch's *t*-test	0.570	—
Fig. 3B	12 hpi	Growth Curve 1: HALo Control vs IFN-β	Welch's *t*-test	0.442	—
Fig. 4B	24 hpi	Growth Curve 1: HALo Control vs IFN-β	Welch's *t*-test	0.301	—
Fig. 4B	0 hpi	Growth Curve 3: HALo Control vs IFN-β Concentration Groups	One-way ANOVA	0.503	$F(3,8) = 0.853$
Fig. 4B	8 hpi	Growth Curve 3: HALo Control vs IFN-β Concentration Groups	One-way ANOVA	0.117	$F(3,19) = 2.235$
Fig. 4B	12 hpi	Growth Curve 3: HALo Control vs IFN-β Concentration Groups	One-way ANOVA	0.524	$F(3,25) = 0.766$
Fig. 4B	24 hpi	Growth Curve 3: HALo Control vs IFN-β Concentration Groups	One-way ANOVA	0.620	$F(3,19) = 0.605$

Table 1. Statistical Analysis of HALo and IFN-β Growth Curve Experiments
Welch's *t-test* and One-way ANOVA were used to conduct the statistical analysis comparison between HALo and Interferon-β over 24 hours. ANOVA statistical values were labeled as F (df_1, df_2). Values $p < 0.05$ were considered statistically significant.

Table 2: Statistical Analysis of NL09 and IFN-β Growth Curve Experiments					
Figure	**Timepoint**	**Comparison**	**Statistical Test**	***p-value***	**Statistic**
Fig. 3D	0 hpi	Growth Curve 1: NL09 Control vs IFN-β	Welch's t-test	0.136	—
Fig. 3D	2 hpi	Growth Curve 1: NL09 Control vs IFN-β	Welch's t-test	0.116	—
Fig. 3D	4 hpi	Growth Curve 1: NL09 Control vs IFN-β	Welch's t-test	0.161	—
Fig. 3D	8 hpi	Growth Curve 1: NL09 Control vs IFN-β	Welch's t-test	0.362	—
Fig. 3D	12 hpi	Growth Curve 1: NL09 Control vs IFN-β	Welch's t-test	0.150	—
Fig. 3D	24 hpi	Growth Curve 1: NL09 Control vs IFN-β	Welch's t-test	0.414	—
Fig. 4D	0 hpi	Growth Curve 3: NL09 Control vs IFN-β Concentration Groups	One way ANOVA	0.735	$F(3,14) = 0.430$
Fig. 4D	8 hpi	Growth Curve 3: NL09 Control vs IFN-β Concentration Groups	One way ANOVA	0.305	$F(3,16) = 1.311$
Fig. 4D	12 hpi	Growth Curve 3: NL09 Control vs IFN-β Concentration Groups	One way ANOVA	0.914	$F(3,14) = 0.172$
Fig. 4D	24 hpi	Growth Curve 3: NL09 Control vs IFN-β Concentration Groups	One way ANOVA	0.517	$F(3,12) = 0.801$

Table 2. Statistical Analysis of NL09 and IFN-β Growth Curve Experiments
Welch's t-test and One-way ANOVA were used to conduct the statistical analysis comparison between NL09 and Interferon-β over 24 hours. ANOVA statistical values were labeled as F (df_1, df_2). Values $p < 0.05$ were considered statistically significant.